Annual Methodological Archive Research Review
http://amresearchreview.com/index.php/Journal/about
Volume 3, Issue 11 (2025)

Online ISSN 3007-3197
Print ISSN 3007-3189

http://amresearchreview.com/index.php/Journal/about

Synthesis and Characterization of Curcuma longa Mediated Cadmium Ferrite for Multifunctional Applications

Sara Ashraf
Department of Physics Islamia University of Bhawalpur
Email: Sarahashraf672@gmail.com

Fatima iqbal
Department of Physics Islamia University of Bhawalpur
Email: fatimaiqbal928@gmail.com

Rabia Ayoub
Department of Physics Islamia University of Bhawalpur
Email: rabiaayoub31@gmail.com

Bazgha Ashraf
Department of Chemistry Islamia University of Bhawalpur
Email: bazghaashraf49@gmail.com

Muhammad shahid khan
Department of Physics Institute of Physics Islamia University of Bhawalpur
Email: mshahid.khan@uo.edu.pk

ABSTRACT

The cadmium ferrite nanoparticles ($CdFe_2O_4$ NPs) prepared by using curcuma longa extract provide hybrid, significant and more functional properties that are difficult to be provided by other ferrites in modern applications and anti-oxidant activities. A co-precipitation process has been adopted due to its simplicity, cost-effectiveness, and ability to produce uniformly sized NPs. The UV-vis absorption spectroscopy, X-ray diffraction spectroscopy, Energy Dispersive X-ray spectroscopy, Fourier transform IR spectroscopy, scanning electron microscopy, and Raman techniques were all used to characterize such produced $CdFe_2O_4$ NPs. Usually, the CdFe2O4 NPs are functional in their morphology and optical behaviors so, here the SEM analysis reveals highly agglomerated, irregular but well-connected grains while the UV-vis absorption spectroscopy indicates the high absorption spectra at 618 nm particularly due to its electronic transitions and shifting of the surface plasmonic resonance (SPR) effect. The XRD pattern indicates the high degree of crystallinity with its peak maxima at (220). All concerned atoms present in this structure were confirmed by EDX specifying the maximum amount of Cd in this ferrites NPs. Additionally, the vibrational modes and structural characteristics of $CdFe_2O_4$ NPs were investigated through FTIR spectroscopic analysis. Usually, water molecules absorb in ferrites structures but the identification of peaks corresponding to Fe-O bonds and hydroxyl

Annual Methodological Archive Research Review
http://amresearchreview.com/index.php/Journal/about
Volume 3, Issue 11 (2025)

Online ISSN 3007-3197
Print ISSN 3007-3189

http://amresearchreview.com/index.php/Journal/about

groups confirms the spinel like structure. The Fe-O bond stretching also confirmed by Raman study which discuss about Fe-O forward stretching and back stretching due to active extract used. The CdFe2O4 NPs shows its demanding and well-defined applications in modern technology. The antioxidant activity, assessed via a spectrophotometric method using DPPH, demonstrated the nanoparticles' potential in biomedical applications because of their ability to donate hydrogen atoms or electrons at different concentrations. The $CdFe_2O_4$ nanoparticles showed strong antibacterial activity against S. aureus and Xanthomonas sp. at 2 mg/disc, and moderate effects on B. subtilis and E. coli. In antifungal tests, A. niger had the highest growth reduction at 1 mg/disc, while Candida albicans showed the lowest at 0.5 mg/disc. The nanoparticles' concentration-dependent inhibition highlights their potential as effective antimicrobial and antifungal agents.

Experimental

Materials

Cadmium nitrate ($Cd(NO_3)_2$ from Sigma Aldrich, Iron (III) nitrate ($Fe(NO_3)_2$) H_2O from Fluka, Distilled water from Aquafina, and Sodium hydroxide (NaOH) from Fluka

Synthesis of Cadmium nitrate ($Cd(NO_3)_2$

Preparation of leaf extract

The synthesis process of the leaf extract is shown in Figure 1. The leaves of Curcuma longa were carefully removed off the plant and collected. After this, leaves cleaned twice through tap water removing for surface contaminants. They were then cleaned through distilled water for leftover impurity. The leaves were cleaned and then cut into little bits. A 250 ml beaker was filled with 30 g of the prepared curcuma longa leaves and 100 ml of DIW. For the purpose of facilitating the extraction process, then it was faced to 80°C. Following the extraction procedure, Whatman-filter paper utilized for filtering the leaf extract via a funnel and a flask with a flat bottom in order to remove the solid residue. To produce a clear and clean leaf extract was the goal of this filtration stage. The leaf extract that was obtained and included the active ingredients was saved for use in the ($CdFe_2O_4$) NP synthesis. In the meanwhile, the filtrate was kept at 4°C in a refrigerator for use in other applications

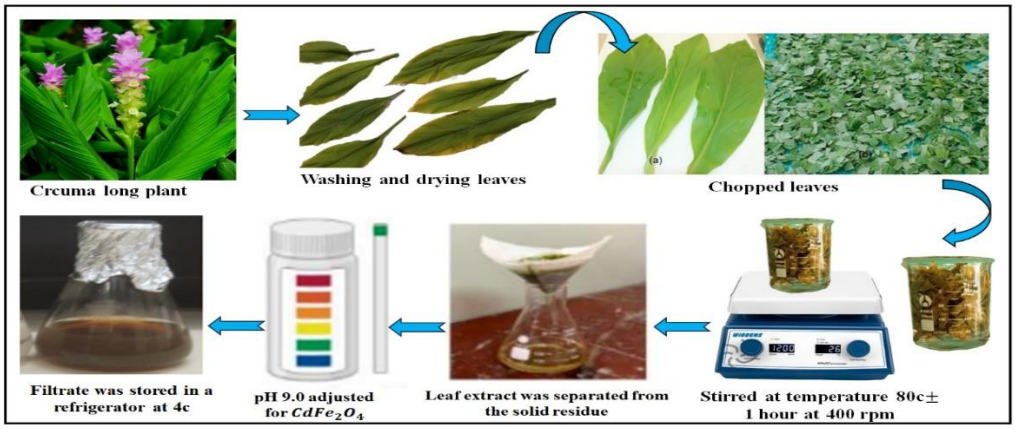


Figure 1 Step by step process of Preparation of leaf extract

Annual Methodological Archive Research Review
http://amresearchreview.com/index.php/Journal/about
Volume 3, Issue 11 (2025)

Online ISSN 3007-3197
Print ISSN 3007-3189

http://amresearchreview.com/index.php/Journal/about

Preparation of Cadmium nitrate (Cd $(NO_3)_2$ nanoparticles

(0.6M) of Fe $(NO_3)^2$ and (0.5M) of cadmium nitrate was dissolved separately in 75 ml of de-ionized water. The resulting Fe $(NO_3)^2$ and cadmium nitrate solutions were mixed together, and was stirred at room temperature (25°C) for 15 minutes. Slowly 25ml of leaf extract produced at pH 9 was added drop by drop to the mixed solution while continuously stirring at 300 rpm, using a magnetic stirrer. Temperature was maintained at 50 ± 2 °C for 6 h during the reaction. The color change of solution was observed from dark yellow to colorless, and dark brown precipitate were obtained, indicating the successful synthesis of cadmium ferrite NPs as shown in Figure 2. The obtained NPs were collected through sedimentation were washed with absolute ethanol, and then performed three additional rinses with milli Q water to remove any unreacted impurities. Finally, the collected NPs were dried at 50 ± 2°C for 6h to obtain the cadmium ferrite NPs in their final form.

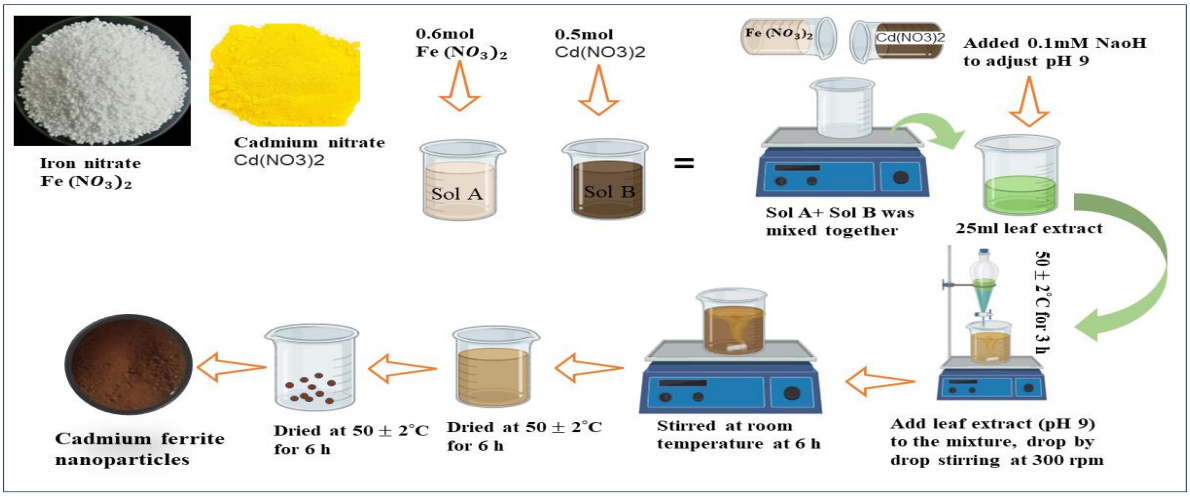


Figure 2 Synthesis process of Cadmium nitrate (Cd $(NO_3)_2$ nanoparticles NPs

Characterizations

Chemical bonding information was obtained using Fourier Transform Infrared Spectroscopy (FTIR) on the Shimadzu IRAffinity-1S, which featured a single reflection diamond ATR accessory. The morphology and elemental composition of the samples were analyzed using Scanning Electron Microscopy (SEM) and Energy-Dispersive X-ray Spectroscopy (EDS) with the FEI Quanta 250 FEG SEM. X-ray Diffraction (XRD) analysis was conducted with the Bruker D8 Advance diffractometer, utilizing Cu-Kα radiation through a monochromatic to determine the crystal structure. Ultraviolet-Visible (UV-Vis) spectroscopy was performed using the Agilent Cary 60 UV-Vis Spectrophotometer to examine the optical properties. Raman spectroscopy, performed with a Renishaw in Via Raman spectrometer, was used to investigate the vibrational modes of the Cd $(NO_3)_2$ nanoparticles (NPs), providing detailed insights into the molecular and structural properties of the samples.

Annual Methodological Archive Research Review
http://amresearchreview.com/index.php/Journal/about
Volume 3, Issue 11 (2025)

Online ISSN 3007-3197
Print ISSN 3007-3189

http://amresearchreview.com/index.php/Journal/about

Antioxidant Activity

The ability of test compounds to donate hydrogen atoms or electrons at concentrations of 50, 75, and 100 µg/mL in methanol was measured using a spectrophotometric assay with DPPH serving as the stable radical reagent in order to evaluate antioxidant activity. The absorbance at 517 nm was measured against a blank after a 30-minute incubation period at room temperature, using ascorbic acid as the standard reference. The formula was used to determine the DPPH free radical scavenging capacity (%).

$$\%\ \text{DPPH scavenging activity} = \left(\frac{A_C - A_S}{A_C}\right) \times 100 \qquad (1)$$

Where A_c is the absorbance of control and A_s is the absorbance in the presence of the samples.

Antimicrobial Activity

To evaluate the antibacterial efficacy of the synthesized samples, both Minimum Inhibitory Concentration (MIC) and zone of inhibition tests were performed using the agar well diffusion method against Gram-positive and Gram-negative bacteria. In Figure (4), nutrient agar plates with a pH of 7.2 were prepared and spread with the bacterial cultures to support their growth. Petri dishes containing solidified agar were inoculated with suspensions of Gram-positive and Gram-negative bacteria. The agar medium was poured aseptically into the plates, allowed to solidify, and then swabbed with fresh bacterial inoculums at approximately 10^6 CFU/mL. The plates were incubated at 37°C for 24 hours. After incubation, the antibacterial activity was assessed by measuring the diameter of the inhibition zones around the wells using a Vernier caliper.

Antifungal Activity

The antifungal activity of synthesized $CdFe_2O_4$ nanoparticles was assessed using the agar disc diffusion method against four fungal strains: A. niger, C. lunata, Rhizopus sp., and Candida albicans. Mueller Hinton Agar (MHA) plates were prepared and spread with the fungal cultures. Sterile wells, created with a cork borer, were used to place sterile discs containing 1 mg of $CdFe_2O_4$ nanoparticles. The spore suspensions of the test fungi were spread onto the agar plates using a bacterial loop, and the plates were allowed to stand for 30 minutes to facilitate the diffusion of any antifungal compounds and fungal growth. Following this, each plate was inoculated with the respective fungal strain to ensure a confluent fungal lawn. Sterile discs with the nanoparticles were then placed on the agar plates using sterile forceps. The plates were incubated at 30°C for 24 hours under visible light. Antifungal activity was measured by the diameter of the zone of inhibition around each disc containing $CdFe_2O_4$ nanoparticles. This zone indicates the area where fungal growth was suppressed due to the antifungal activity of the nanoparticles.

The percentage inhibition of fungal growth relative to the control was calculated using the formula:

$$\text{Antifungal Index (AI)} = \left(1 - \frac{D_a}{D_b}\right) \times 100 \qquad (2)$$

D_a: Diameter of fungal growth in treated dishes (mm)
D_b: Diameter of fungal growth in control dishes (mm)

Annual Methodological Archive Research Review
http://amresearchreview.com/index.php/Journal/about
Volume 3, Issue 11 (2025)

Online ISSN 3007-3197
Print ISSN 3007-3189

http://amresearchreview.com/index.php/Journal/about

Result and Discussion

Optical Properties

Usually, UV-vis absorption spectrum for $CdFe_2O_4$ NPs occurs in the wide range 200 nm to 800 nm or more, depending on the particle size and the reaction kinetics being analyzed (Surendra et al., 2024). In order to examine the optical characteristics and band gap of the nanoparticles, it is necessary to cover the pertinent electronic transitions and absorption edges within this range. It is possible to examine the material's specific absorption at 618 nm for electronic transitions, which will reveal important details about its electronic structure. The sharpest peak represented by a blue curved in Figure 3 (a) is occurring at 618 nm, which verifies formation of cubic $CdFe_2O_4$ NPs (Patil et al., 2020). It provides important insights into their optical characteristics, especially their band gap energy and electronic structure (Yassine et al., 2023). The absorption peak at 618 nm indicates particular electronic transitions in the substance. This peak may be caused by charge transfer transitions between the Fe^{+3} ions or by d-d transitions of Fe ions in the octahedral sites of the spinel structure and O^{-2} ions. Strong interaction between the incident photons and the electronic states of the nanoparticles is indicated by the presence of this peak, indicating potential uses of the nanoparticles in sensors, optoelectronic devices, and photocatalysis. The absorption edge in the UV-Vis spectrum also provides an estimate of the optical band gap (Patil et al., 2024), an important parameter to determine the suitability of $CdFe_2O_4$ NPs in different technological applications. Knowledge of these optical properties is crucial for customizing the nanoparticles for particular purposes, like increasing their photocatalytic efficiency or making the most of their use in solar energy conversion systems.

Structure

The crystal structure of $CdFe_2O_4$ NPs confirmed by XRD technique

Figure 3 (b) **S**hows XRD pattern with a sharp peak (220) indicating the highly oriented growth of the sample containing $CdFe_2O_4$ NPs and its peaks detected at 2θ=23.115, 29.3, 38.83.9, 44.26, 48.18, 56.24, 61.86, 64.69, 77.60, on level surface (111), (220), (222), (311), (420), (400), (440), (331), (511), (440), (531) and (622) with lattice constant 8.69 Å. These peaks are well-resolved and sharp, indicating good crystallinity of the nanoparticles (Ismail et al., 2013). The crystallite size was determined using Debye Scherrer's equation. The broadening of Bragg's peaks confirms formation of the NPs (Narayanan & Sakthivel, 2008). These peaks' existence attests to the high degree of crystallinity at which the cadmium ferrites phase formed. The sharp peak found at $2\theta = 29.1°$, which corresponds to the (220) plane, suggests that the nanoparticles are growing in a highly oriented manner along this crystallographic direction. It is possible to attribute this preferential orientation to the particular synthesis conditions that support anisotropic growth. The synthesis of phase-pure $CdFe_2O_4$ NPs was successfully verified, as evidenced by the calculated lattice constant of approximately 8.69 Å for the $CdFe_2O_4$ NPs, which is consistent with reported values for this material. Furthermore, the lack of any extra peaks in the

Annual Methodological Archive Research Review
http://amresearchreview.com/index.php/Journal/about
Volume 3, Issue 11 (2025)

Online ISSN 3007-3197
Print ISSN 3007-3189
http://amresearchreview.com/index.php/Journal/about

XRD pattern shows that there are no impurities or secondary phases present in the produced NPs (Kolekar).The average crystallite size of the $CdFe_2O_4$ NPs was calculated using the Scherrer equation to be roughly 40.9 nm also well reported in literature (Baghayeri et al., 2018). The final structure of $CdFe_2O_4$ NPs is a cubic spinel structure (JCPDS card No. 22-1063). This nanoscale dimension reflects the synthetic material's fine particle nature, which may impart special chemical and physical properties appropriate for a range of uses.

Morphology and Elemental Composition

The confirmation of NPs can be done by `q` analyzing the sample with energy dispersive X-ray spectroscopy. The EDS confirms the constituents of $CdFe_2O_4$ NPs sample as shown in Figure 3 (c). Such spectra in the figure shows the prominent peak of cadmium and there exhibit a very small peak of Fe confirming the formation of Cadmium ferrites. The small traces of Fe describe that Fe $(NO_3)_2$ have been used as a pre-curser in the reaction so, herein Fe is detected in very small amount. The graph reveals that second prominent peak is of O showing the oxidation in the moisture. The above spectrum specify that cadmium is present in large amount in the sample confirming the formation $CdFe_2O_4$ NPs. SEM images of the prepared $CdFe_2O_4$ NPs shown in Figure 3 (d). These are magnified at various scale to check its internal structure and morphology. The synthesized NPs were in nanometer scale with an average size of 36 nm as shown in Figure 3 (d). Images obtained by scanning electron microscopy (SEM) when examined at 2.08, 4.15, and 10.4 µm, nanoparticles reveal intricate details about their morphology and structure. The shape, size distribution, surface texture, and pore presence of the nanoparticles are all revealed by the SEM analysis. The $CdFe_2O_4$ NPs have an approximately spherical form with some degree of imperfection. The synthesis method used may be the cause of this irregularity, as it can result in non-uniform growth rates and shape variations. For a variety of applications, the roughly spherical morphology is advantageous because It can raise the ratio of surface area to volume, which is necessary for catalysis and adsorption. The material (Curcuma longa and $CdFe_2O_4$ extracts) has a textured surface with unique characteristics at both the macro and nano scales, according to the SEM analysis. These observations underscore the significance of thorough surface analysis in material science and engineering by characterizing the material's physical state and offering insights into its potential for a range of applications.

Raman Spectroscopy

Figure 3 (e) shows the Surface-enhanced Raman scattering (SERS) of $CdFe_2O_4$ (cadmium ferrite) reveals critical molecular vibrations, such as the Fe-O bond stretching (Cozar et al., 2006; Mikoliunaite et al., 2023) at 1055 cm^{-1} and a smaller peak at 723 cm^{-1}, indicating Fe-O bond bending. Ferrite nanoparticles enhance the effect and provide detailed insights into $CdFe_2O_4$'s structural and electronic properties. Understanding low-frequency phonon modes and vibrational properties is critical for future applications in catalysis, sensors, and magnetic materials. Curcuma longa's bioactive compounds function as reducing and stabilizing agents, resulting in nanoparticles with improved surface properties. These biogenic nanoparticles exhibit increased SERS activity, allowing for more in-depth analysis of surface interactions

Annual Methodological Archive Research Review
http://amresearchreview.com/index.php/Journal/about
Volume 3, Issue 11 (2025)

Online ISSN 3007-3197
Print ISSN 3007-3189

http://amresearchreview.com/index.php/Journal/about

and molecular vibrations.

Vibrational Analysis

Figure 3 (f) shows the FTIR spectra of $CdFe_2O_4$ NPs provide valuable insights into the vibrational modes and structural characteristics of the material (Vishnu et al., 2023). The identification of peaks corresponding to Fe-O bonds and hydroxyl groups confirms the formation of the spinel structure (Rajeevgandhi et al., 2020) and the presence of surface adsorbed species. From the IR spectrum of $CdFe_2O_4$, the peak at 831 cm^{-1}corresponds to the stretching vibrations of the Fe-O bonds in the tetrahedral sites (Naseri et al., 2016) of the spinel structure. The presence of this peak confirms the formation of the spinel ferrite phase. The hydroxyl groups (OH) adsorbed on the surface of the $CdFe_2O_4$ particles are responsible for the peak at 1334 cm^{-1}. In ferrite materials, water molecules frequently adsorb. However, the stretching vibrations of C=O bonds are linked to the peak at 1793 cm^{-1} observed at this frequency, which may be the result of organic contaminants or leftover solvents used during the synthesis process (Heryanto et al., 2023). Less frequently occurring, another weak spot at 2429 cm^{-1} might be associated with the fundamental vibrations' overtone or combination bands. To determine the precise origin, more investigation and comparison with existing literature are required. Lastly, a peak measuring 3384 cm^{-1}.The presence of moisture or hydroxyl groups on the surface of the ferrite material is indicated by the broad peak at this frequency, which is typical of O-H stretching vibrations.

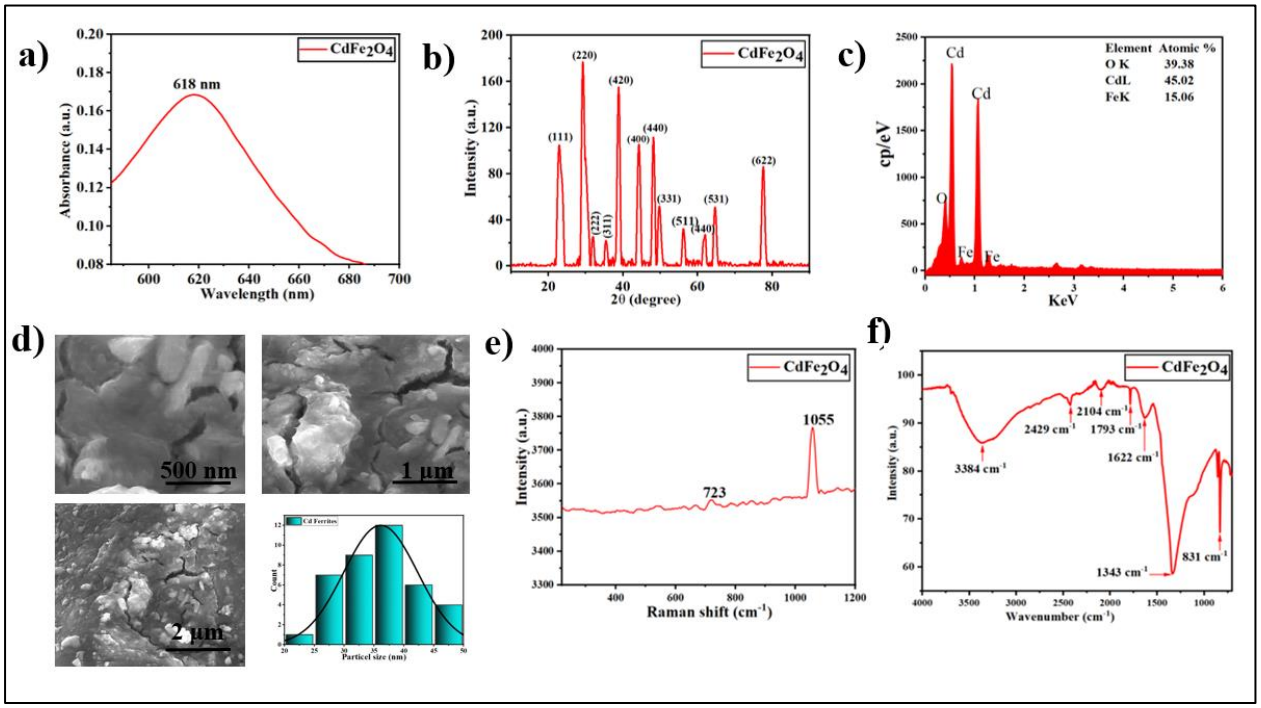


Figure 3 UV-vis absorption spectrum, XRD pattern, EDS spectrum for elemental composition, SEM analysis for morphology and particle size distribution, SERS study, and FTIR spectra of $CdFe_2O_4$ nanoparticles (NPs).

Annual Methodological Archive Research Review
http://amresearchreview.com/index.php/Journal/about
Volume 3, Issue 11 (2025)

Online ISSN 3007-3197
Print ISSN 3007-3189

http://amresearchreview.com/index.php/Journal/about

Antioxidant activity of Cadmium Ferrite Nanoparticles of extract of curcuma longa

Figure 4 shows the $CdFe_2O_4$ NPs exhibited a concentration-dependent antioxidant effect, as evident from the observed percentage inhibitions of free radical production from DPPH. The percentage restrictions on the production of free radicals from DPPH demonstrated that the antioxidant activity of the $CdFe_2O_4$ NPs depended on their capacity to concentrate. The degree of inhibition shown by $CdFe_2O_4$ was 62.54% at 50 µg/mL, improving to 67.89% at 75 µg/mL and 79.9% at 100 µg/mL. Curcuma longa, on the other hand, showed a restriction of 77.27% at 50 µg/mL, improving to 80.9% at 75 µg/mL, and peaking at 85% at 100 µg/mL.The traditional Microorganisms Concentrations, on the other hand, are 10 (µg/mL), 20 (µg/mL), 25 (µg/mL), and 15 (µg/mL). At 50 µg/mL, ascorbic acid exhibited an inhibition of 81.23%; at 75 µg/mL, it increased to 83.17%, and at 100 µg/mL, to 88.36%. These results imply that $CdFe_2O_4$ NPs might possess antioxidant qualities. The proportion of inhibitory activity and the quantity of $CdFe_2O_4$ NPs were shown to be positively correlated. This pattern demonstrates how well the NPs scavenge DPPH free radicals, lowering their potential to cause oxidative damage. These results are consistent with the hypothesis that $CdFe_2O_4$ NPs have potential as antioxidants, as they show that their efficiency varies with quantity. Table 1 shows the percentage inhibition of DPPH radical production by $CdFe_2O_4$ NPs, Curcuma longa and ascorbic acid at different concentrations. As the concentration increases, the percentage inhibition also increases for the compounds.

Table 1 The outcomes of Synthesized Cd ferrites Antioxidant Activity

Compound	**50 µg/mL (%)**	**75 µg/mL (%)**	**100 µg/mL (%)**
$CdFe_2O_4$	62.54	67.89	79.99
curcuma longa	77.27	80.9	85
Ascorbic acid	81.23	83.17	88.36

Annual Methodological Archive Research Review
http://amresearchreview.com/index.php/Journal/about
Volume 3, Issue 11 (2025)

Online ISSN 3007-3197
Print ISSN 3007-3189

http://amresearchreview.com/index.php/Journal/about

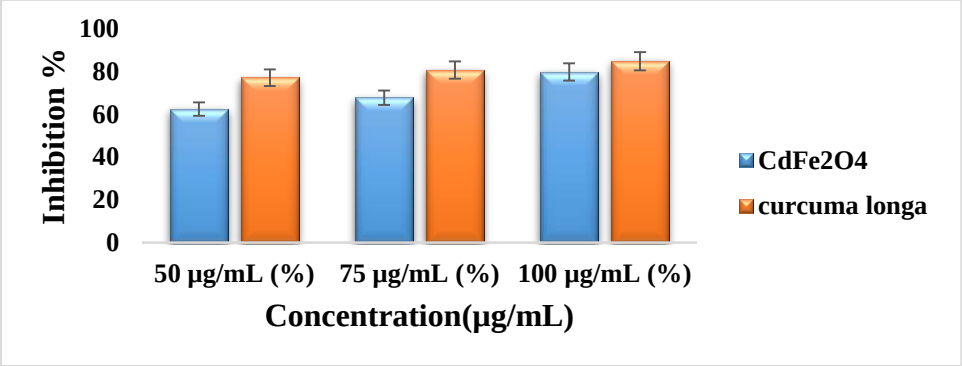


Figure 4 Antioxidant Activity of Cadmium ferrite ($CdFe_2O_4$)

Antimicrobial potential of Cadmium Ferrite Nanoparticles of extract of curcuma longa

Figure 5 presents the statistical findings on the strontium oxide nanoparticles' antibacterial capability from the methanolic crude fractions derived from curcuma longa roots. According to experimental findings, S. aureus had the largest zone of inhibition (69.8%) in response to curcuma longa Cadmium ferrite nanoparticles at a dosage of 2 mg disc-1. Xanthomonas sp. displayed the same concentration with a value of 61.9%. S. aureus demonstrated the third highest result of inhibition (59.9%) at a dosage of 1 mg disc-1. For E. coli, the minimal inhibitory zone (39.31%) was seen at a dose of 0.5 mg disc-1. According to the statistical study, B. subtilis and E. coli showed only moderate sensitivity to the nanoparticles, whereas S. aureus and Xanthomonas showed good sensitivity.

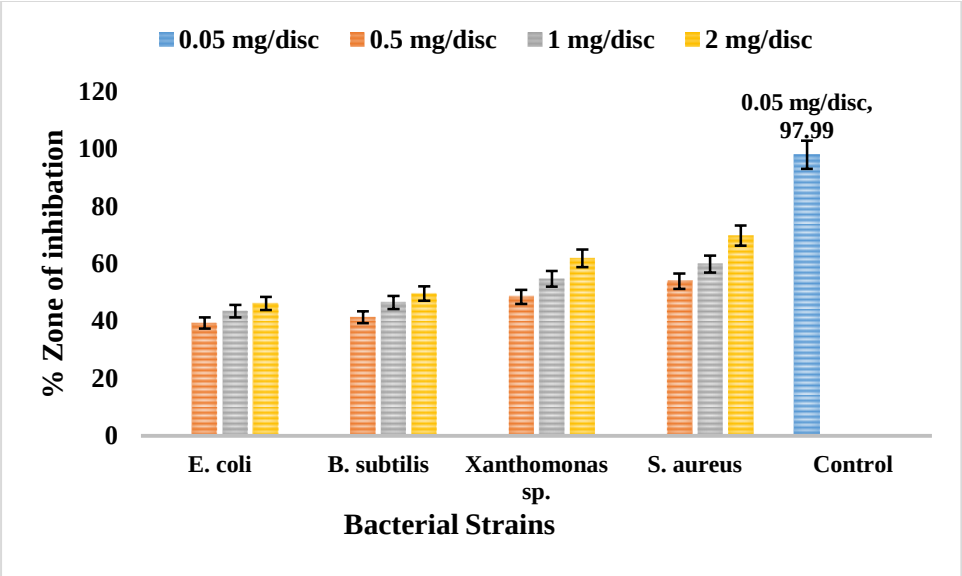


Figure 5 Antimicrobial potential, with Standard deviation of Cadmium ferrite NPs of extract of curcuma longa against five bacterial strains by using disc diffusion method

Annual Methodological Archive Research Review
http://amresearchreview.com/index.php/Journal/about
Volume 3, Issue 11 (2025)

Online ISSN 3007-3197
Print ISSN 3007-3189

http://amresearchreview.com/index.php/Journal/about

Table 2 Zone of Inhibitions Cadmium ferrite NPs

Bacteria Strain	0.05 mg/disc	0.5 mg/disc	1 mg/disc	2 mg/disc
E. coli		39.31	43.43	46.16
B. subtilis		41.32	46.5	49.6
Xanthomonas sp.		48.45	54.7	61.9
S. aureus		53.88	59.9	69.8
Control	97.99			

Antifungal potential of Cadmium ferrite NPs of extract of curcuma longa

The antifungal activity of nanoparticles derived from curcuma longa aqueous extract is depicted in Figure 6. Considering the whole set of findings, it was evident that the leaves' extracted nanoparticles (NPs) could effectively inhibit the growth of every strain. The growth of the microscopic creature decreased as the concentration of the nanoparticles increased. When comparing the growth of the extracts and controls, A. niger (91%) was shown to have the greatest growth reduction (91%), with a concentration of 1 mg disc-1. Rhizopus and Curvularia both shown a noteworthy degree of antifungal activity. At 0.5 disc-1 concentration, the lowest growth inhibition value of 25% was reported for Candida albicans.

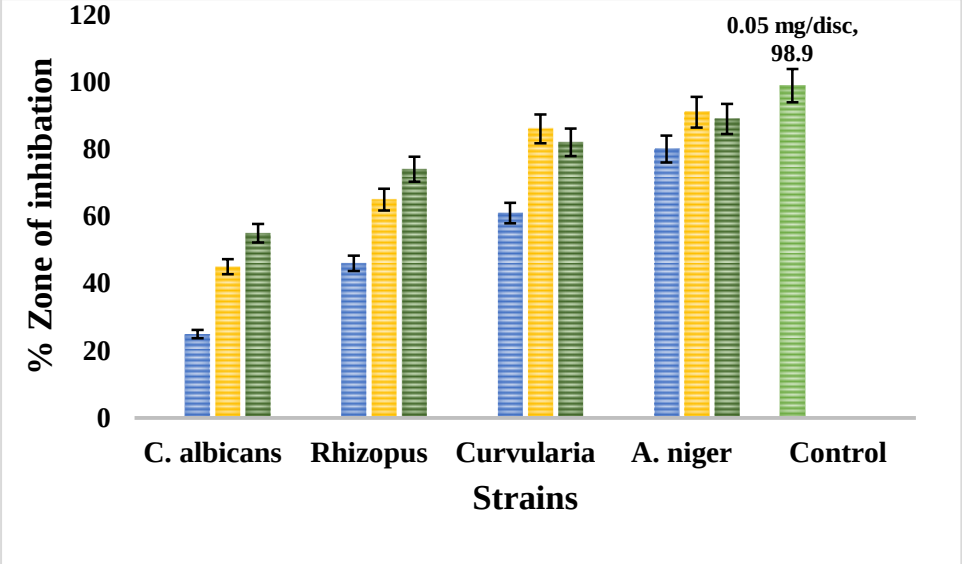


Figure 6 Antifungal potential, with Standard deviation of Cadmium ferrite NPs of extract of curcuma longa against four fungal and one yeast strain through well diffusion method

Annual Methodological Archive Research Review
http://amresearchreview.com/index.php/Journal/about
Volume 3, Issue 11 (2025)

Online ISSN 3007-3197
Print ISSN 3007-3189

http://amresearchreview.com/index.php/Journal/about

Table 3 Zone of inhibitions at different concentrations

Bacteria Strain	0.05 mg/disc	0.5 mg/disc	1 mg/disc	2 mg/disc
C. albicans		25	45	55
Rhizopus		46	65	74
Curvularia		61	86	82
A. niger		80	91	89
Control	98.9			

Photocatalytic performance of $CdFe_2O_4$ nanoparticles

The impact of contact time on the degradation of Reactive Blue 13 dye was studied within 0-60 min time intervals, as shown in Fig 1(a). It is evident from the graph provided that time and the percentage decolorization of Reactive Blue 13 dye using $CdFe_2O_4$ nanoparticles is directly proportional to each other. First of all, degree of decolorizing is 30% and during the first 10 minutes quickly grows and becomes 55%. This suggests that at the early stages of the process there was a very fast rate of degradation probably because the number of dye molecules as well as the number of active photocatalytic sites on the nanoparticles was high. After 10-30 min phase of reaction, the decolorization rate decreases, whereas about 75% of the dye was decolorized at 30 min. It also implies that for lower dye concentration the rate of degradation is also low. perpetual: continually advancing, in the last stage from 30 to 60 minutes the decolorization rate rises progressively but with less intensity refining up to a reach ninety percent decolorization rate. This points out that although most of the dye molecules have been broken down the rate is rather slow towards the end perhaps because there are fewer reactive species or dye molecules. In sum, the graph has depicted that $CdFe_2O_4$ nanoparticles exhibit suitable photodegradation activities of the dye most of the decolorization happened in the initial 30 min.

The performance of photodegradation of Reactive Blue 13 dye by using $CdFe_2O_4$ nanoparticles on varying pH is evidenced from the Fig 1(b). that exhibits a sharp decrease in degradation percent from pH 2 to 14. The highest value of degradation efficiency is observed when the solution is the most acidic, that is at pH 2 and the values drops to 90.77% while those at pH 7 and 9 are 45.77% and 25.59% respectively. This increased degradation is ascribed to oxygenic anion radicals that are formed by the reaction of oxygen molecules with the electron of the $CdFe_2O_4$ photocatalyst. The degradation efficiency decreases with the increase in pH, likely because the nanoparticles have a negative charge and there is electrostatic repulsion between the anionic nanoparticles and the anionic Reactive Blue 13. This repulsion lowers the number of dye molecules that the catalyst is able to interface with and degrade. Similarly, owing to the action OH• radicals with Cl^- anions at higher pH, HCl treatment results the generation of ClO^- • anions. These ClO^- • species do not

Annual Methodological Archive Research Review
http://amresearchreview.com/index.php/Journal/about
Volume 3, Issue 11 (2025)

Online ISSN 3007-3197
Print ISSN 3007-3189

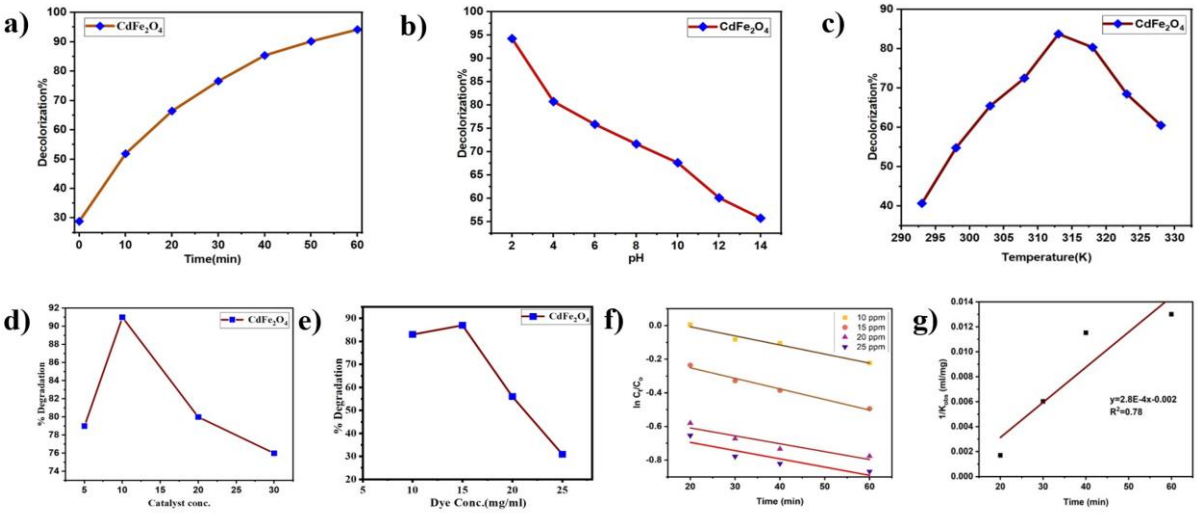
http://amresearchreview.com/index.php/Journal/about

act in breaking the dye, which reduces the efficiency as the pH rises. Therefore, the percentage of dye degraded decreases sharply once the pH is raised above 2 from the pH scale as represented in the graph.

From Fig 1(c) the range between 290 K to around 315 K the decolorization percentage rises gradually to about 80%. This might be as a result of improved molecular interactions at higher temperatures than at lower temperatures. However, the efficiency of decolorization decreases at temperatures higher than 315 K and at 325 K is approximately 60%. This reduction may be attributed to events such as electron-hole recombination or even reduced interaction between dye molecules and the catalyst at higher temperatures. Therefore, the maximum photocatalytic degradation is achievable at 315 K.

In the Fig 2(a), the catalyst concentration ranges from 5 to 30 mg, and the degradation percentage increases until it reaches a maximum at 10 mg of catalyst concentration, where approximately 92% degradation occurs. Beyond this point, the degradation percentage decreases with further increases in catalyst concentration. This trend can be explained by the increase in surface area with rising catalyst dosage, which enhances photocatalytic activity up to a certain point. However, at higher concentrations, agglomeration of catalyst particles and increased turbidity can obstruct sunlight penetration, thereby reducing photocatalytic efficiency.

As shown in Fig 2(b), the dye concentration ranges from 10 to 25 mg/ml, with the maximum degradation occurring at 15 mg/ml, showing a degradation percentage of approximately 90%. As the dye concentration increases beyond 15 mg/ml, the degradation efficiency decreases sharply. This decline is due to the excessive amount of dye molecules, which hinder their interaction with the catalyst and sunlight, thereby reducing the photocatalytic degradation process. Higher dye concentrations also reduce the path length of incoming photons, which limits the amount of sunlight reaching the catalyst surface, further lowering the degradation efficiency.



Annual Methodological Archive Research Review
http://amresearchreview.com/index.php/Journal/about
Volume 3, Issue 11 (2025)

Online ISSN 3007-3197
Print ISSN 3007-3189
http://amresearchreview.com/index.php/Journal/about

Degradation kinetics

Photocatalytic ability of Reactive Blue 13 dye under sunlight irradiation was evaluated using the Reactive Blue 13 dye as a model compound. Two kinetic models were used to analyze the degradation process: the L-H model and the first-order reaction model are used in the framework of Figs 3 (a, b). Equation (1) is showing first order reaction analysis of the decolorization of the Reactive Blue 13 dye under sunlight.

$$\frac{-dc}{dt} = k_1(1 - \exp[-k_2 c_o])\left[\frac{c}{c_o}\right] = kc \qquad (1)$$

The first-order model was further verified by working with the natural logarithm of the initial concentration to the time dependent concentration ratio ($\ln(C_0 /Ct)$). If this plot extends into a straight line this will indicate that the first-order model holds true for the reaction kinetics The Equation 2 shows the L-H kinetic model that was employed to describe the photocatalytic degradation process.

$$\ln(\frac{C_t}{C_o}) = -k_{obs}t \qquad (2)$$

Here, C_t represents the concentration of Reactive Blue 13 dye at a specific time point (t), while C_0 signifies its initial concentration. The rate constant of the reaction is denoted by k. We determined the rate constant by analyzing the graph between $\ln(C/C_0)$ and time for various Reactive Blue 13 dye concentrations. Furthermore, a plot was constructed between the inverse of the apparent rate constant ($1/K_{obs}$) and the initial concentration (C_0) to represent the L-H model, as shown in Fig.

By analyzing the data obtained, it can be concluded that pseudo - first order kinetics seems to be the most effective method for the degradation of Reactive Blue 13 dye by using cadmium ferrites NPs.

Mechanism of dye degradation

Active species involved in the photodegradation of Reactive Blue 13 dye using, the synthesized $CdFe_2O_4$ nanoparticles were super oxide radicals, hydroxyl radicals and electrons in addition to holes. Upon photo illumination electron hole pairs are created in the system, where electrons are in the conduction band (CB) while the holes are in the valence band (VB). The holes promote the oxidation of water and formation of hydroxyl radicals whereas the electrons reduce molecular oxygen to form the superoxide radicals. These radicals have the noble responsibility of decomposing dye molecules into other forms such as mineral acids of water and carbon di-oxide. It extremely depends on the pH since surface charges of the nanoparticles are altered with the change in pH, which in turn defines the interaction with the dye molecules. Electrons and holes both help in formation of reactive species which creates oxidation and reduction of dye molecules.

$$\text{Photocatalyst} + h\upsilon \rightarrow e^-_{C.B} + h^+_{V.B}$$
$$H_2O + h^+_{V.B} \rightarrow OH^{\cdot} + H^+$$
$$O_2 + e^-_{C.B} \rightarrow O^{-2}$$
$$O^{-2} + H^+ \rightarrow HO^{\cdot}_2$$
$$2HO^{\cdot}_2 \rightarrow O_2 + H_2O_2$$
$$H_2O_2 \rightarrow 2OH^-$$
$$\text{Reactive blue 13 Dye} + OH^- \rightarrow H_2O + CO_2$$

Annual Methodological Archive Research Review
http://amresearchreview.com/index.php/Journal/about
Volume 3, Issue 11 (2025)

Online ISSN 3007-3197
Print ISSN 3007-3189

http://amresearchreview.com/index.php/Journal/about

Conclusion

In this study, cadmium ferrite nanoparticles ($CdFe_2O_4$ NPs) were synthesized via co-precipitation method. Curcuma longa extract has improved the synthesis and characterization of $CdFe_2O_4$ NPs, resulting in significant advancements in their understanding and application. Herein, the scanning electron microscopy (SEM) analysis revealed a textured surface with distinct macro and nanoscale characteristics, highlighting the significance of detailed surface analysis in advance materials. The nanoparticles formed agglomerates with an average size of 36 nm, as previously reported. While, the UV-vis absorption spectrum of $CdFe_2O_4$ NPs spanned a broad range from 200 nm to 800 nm, which is influenced by particle size and reaction kinetics. Additionally, Surface-enhanced Raman scattering (SERS) revealed the molecular vibrations of $CdFe_2O_4$, including Fe-O bond stretching at 1055 cm^{-1} and bending at 723 cm^{-1}. These observations confirm the formation of the spinel structure and the presence of surface-adsorption species, validating the material's structural and electronic properties. The XRD pattern indicates the high degree of crystallinity with its peak maxima at (220). FTIR indicates the identification of peaks corresponding to Fe-O bonds and hydroxyl groups confirms the formation of the spinel structure. The $CdFe_2O_4$ NPs demonstrated strong antioxidant activity, with up to 79.9% inhibition of free radicals, and exhibited significant antibacterial effects against S. aureus and Xanthomonas sp., as well as notable antifungal activity against A. niger. These findings highlight the potential of $CdFe_2O_4$ NPs for diverse applications in biomedical and technological fields, underscoring their versatility and effectiveness. The comprehensive surface analysis and characterization techniques employed in this research offer valuable insights into the physical state and potential applications of $CdFe_2O_4$ NPs, paving the way for future advancements in material science and engineering.

Reference

Baghayeri, M., Amiri, A., Maleki, B., Alizadeh, Z., & Reiser, O. (2018). A simple approach for simultaneous detection of cadmium (II) and lead (II) based on glutathione coated magnetic nanoparticles as a highly selective electrochemical probe. Sensors and Actuators B: Chemical, 273, 1442-1450.

Cozar, O., Leopold, N., Jelic, C., Chiş, V., David, L., Mocanu, A., & Tomoaia-Cotişel, M. (2006). IR, Raman and surface-enhanced Raman study of desferrioxamine B and its Fe (III) complex, ferrioxamine B. Journal of Molecular Structure, 788(1-3), 1-6.

Heryanto, H., Siswanto, S., Rahmat, R., Sulieman, A., Bradley, D. A., & Tahir, D. (2023). Nickel Slag/laterite soil and nickel slag/iron sand nanocomposites: structural, optical, and electromagnetic absorption properties. ACS Omega, 8(21), 18591-18602.

Ismail, S., Labib, S., & Attallah, S. (2013). Preparation and Characterization of Nano- Cadmium Ferrite. Journal of Ceramics, 2013(1), 526434.

Kolekar, Y. MAGNETISM AND MAGNETIC PROPERTIES OF MATERIALS: A CASE STUDY. Bhumi Publishing, Nigave Khalasa, Kolhapur 416207, Maharashtra, India Website: www. bhumipublishing. com E-mail:

Online ISSN 3007-3197
Print ISSN 3007-3189

bhumipublishing@ gmail. com, 11.

Mikoliunaite, L., Stankevičius, E., Adomavičiūtė-Grabusovė, S., Petrikaitė, V., Trusovas, R., Talaikis, M., Skapas, M., Zdaniauskienė, A., Selskis, A., & Šablinskas, V. (2023). Magneto-plasmonic nanoparticles generated by laser ablation of layered fe/au and fe/au/fe composite films for sers application. Coatings, 13(9), 1523.

Narayanan, K. B., & Sakthivel, N. (2008). Coriander leaf mediated biosynthesis of gold nanoparticles. Materials Letters, 62(30), 4588-4590.

Naseri, M., Naderi, E., & Saion, E. (2016). The Study of Properties of the Ferrite Nanoparticles Synthesized by Thermal Treatment Method. Nanoscale, 3(1).

Patil, R. P., Teli, S. B., Gophane, A., Patil, A. R., Kadam, J. J., Kamble, P. D., & Garadkar, K. M. (2024). Biogenic CdFe2O4 nanorods for sunlight-assisted photodegradation and cytotoxicity study. Research on Chemical Intermediates, 50(5), 2267-2289.

Patil, S., Anantharaju, K., Rangappa, D., Vidya, Y., Sharma, S., Renuka, L., & Nagabhushana, H. (2020). Magnetic Eu-doped MgFe2O4 nanomaterials: an investigation of their structural, optical and enhanced visible-light-driven photocatalytic performance. Environmental Nanotechnology, Monitoring & Management, 13, 100268.

Rajeevgandhi, C., Bharanidharan, S., Savithiri, S., Guganathan, L., Sugumar, P., Sathiyamurthy, K., & Mohan, K. (2020). Synthesis, characterizations and quantum chemical calculations of the spinel structure of Fe 3 O 4 nanoparticles. Journal of Materials Science: Materials in Electronics, 31, 21419-21430.

Surendra, B., Harish, K., Kiran, T., Shanbhag, V. V., & Khasim, S. (2024). Effect of modified CdFe2O4 NPs-graphite-based electrochemical sensor for heavy metal lead with paracetamol detection and photocatalytic applications. Journal of Materials Science: Materials in Electronics, 35(18), 1252.

Vishnu, G., Singh, S., Naik, T. S. K., Viswanath, R., Ramamurthy, P. C., Bhadrecha, P., Naik, H. B., Singh, J., Khan, N. A., & Zahmatkesh, S. (2023). Photodegradation of methylene blue dye using light driven photocatalyst-green cobalt doped cadmium ferrite nanoparticles as antibacterial agents. Journal of Cleaner Production, 404, 136977.

Yassine, R., Abdallah, A., Hassan, R. S., Yaacoub, N., Awad, R., & Bitar, Z. (2023). Prospecting the structural and magnetic features of (x) CuO/(1-x) CdFe2O4 nanocomposite system (0.0≤ x≤ 1.0). Journal of Nanoparticle Research, 25(5), 90.